

FedProf: Selective Federated Learning with Representation Profiling

Wentai Wu, Ligang He, Weiwei Lin, and Carsten Maple *

Abstract

Federated Learning (FL) has shown great potential as a privacy-preserving solution to learning from decentralized data that are only accessible to end devices (i.e., clients). In many scenarios, however, a large proportion of the clients are probably in possession of low-quality data that are biased, noisy or even irrelevant. As a result, they could significantly slow down the convergence of the global model we aim to build and also compromise its quality. In light of this, we propose FEDPROF, a novel algorithm for optimizing FL under such circumstances without breaching data privacy. The key of our approach is a distributional representation profiling and matching scheme that uses the global model to dynamically profile data representations and allows for low-cost, lightweight representation matching. Based on the scheme we adaptively score each client and adjust its participation probability so as to mitigate the impact of low-value clients on the training process. We have conducted extensive experiments on public datasets using various FL settings. The results show that the selective behaviour of our algorithm leads to a significant reduction in the number of communication rounds and the amount of time (up to $2.4\times$ speedup) for the global model to converge and also provides accuracy gain.

1 Introduction

With the advances in Artificial Intelligence (AI), we are seeing a rapid growth in the number of AI-driven applications as well as the volume of data required to train them. However, a large proportion of data used for machine learning are often generated outside the data centers by distributed resources such as mobile phones and IoT (Internet of Things) devices. It is predicted that the data generated by IoT devices will account for 75% of the total in 2025 [1]. Under this circumstance, it will be very costly to gather all the data for centralized training. More importantly, moving the data out of their local devices (e.g., mobile phones) is now restricted by law in many countries, such as the General Data Protection Regulation (GDPR)¹ enforced in EU.

We face three main difficulties to learn from decentralized data: i) massive scale of end devices; ii) limited communication bandwidth at the network edge; and iii) uncertain data distribution and data quality. As a promising solution, Federated Learning (FL) [2] is a framework for efficient distributed machine learning with privacy protection (i.e., no data exchange). A typical process of FL is organized in rounds where the devices (clients) download the global model from the server, perform local training on their data and then upload their updated local models to the server for aggregation. Compared to traditional distributed learning methods, FL is naturally more communication-efficient at scale [3, 4]. Nonetheless, several issues stand out.

*W. Wu, L. He (corresponding author, ligang.he@warwick.ac.uk) are with the Department of Computer Science, University of Warwick. W. Lin is with the School of Computer Science and Engineering, South China University of Technology. C. Maple is with Warwick Manufacturing Group (WMG), University of Warwick.

¹<https://gdpr.eu/what-is-gdpr/>

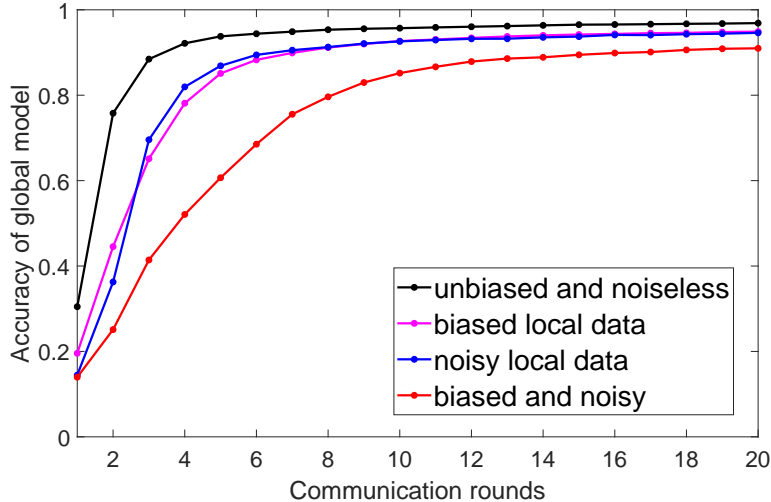


Figure 1: (Preliminary experiment) The global model’s convergence on different data conditions. We ran the FL process with 100 clients to learn a CNN model on the MNIST dataset, which is partitioned and allocated to clients in four different ways where the data are 1) *original* (black line): noiseless and evenly distributed across the clients, 2) *biased* (magenta line): locally class-imbalanced, 3) *noisy* (blue line): blended with noise, or 4) *biased and noisy* (red line). The noise (if applied) covers 65% of the clients; the dominant class accounts for >50% of the samples for biased local data. The fraction of selected clients is 0.3 for each round.

1.1 Motivation

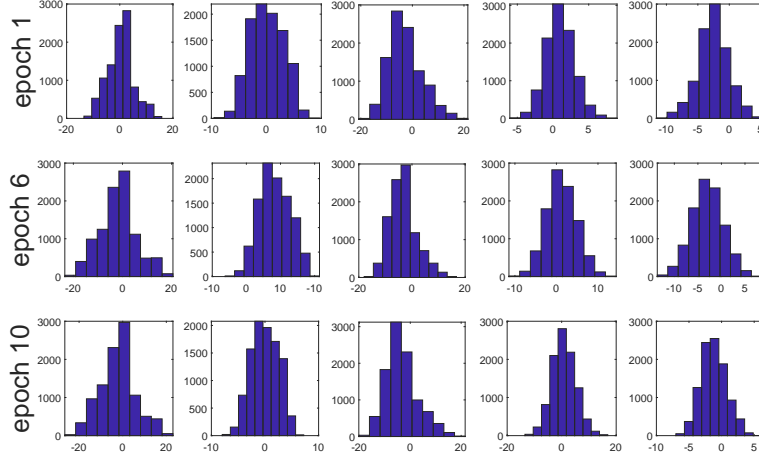
1) *FL is susceptible to biased and low-quality local data.* Only a fraction of clients are selected for a round of FL (involving too many clients leads to diminishing gains [5]). The standard FL algorithm [2] selects clients randomly, which implies that every client (and its local data) is considered equally important. This makes the training process susceptible to local data with strong heterogeneity and of low quality (e.g., user-generated texts [6] and noisy photos). In some scenarios, local data may contain irrelevant or even adversarial samples [7, 8] from malicious clients [9, 8, 10]. Traditional solutions such as data augmentation [11] and re-sampling [12] prove useful for centralised training but applying them to local datasets may introduce extra noise [13] and increase the risk of information leakage [14]. Another naive solution is to directly exclude those low-value clients with low-quality data, which, however, is often impractical because i) the quality of the data depends on the learning task and is difficult to gauge; ii) some noisy or biased data could be useful to the training at early stages [15]; and iii) sometimes low-quality data are very common across the clients.

In Fig. 1 we demonstrate the impact of involving “low-value” clients by running FL over 100 clients to learn a CNN model on MNIST using the standard FEDAVG algorithm. From the traces we can see that training over clients with problematic or strongly biased data can compromise the efficiency and efficacy of FL, resulting in an inferior global model that takes more rounds to converge.

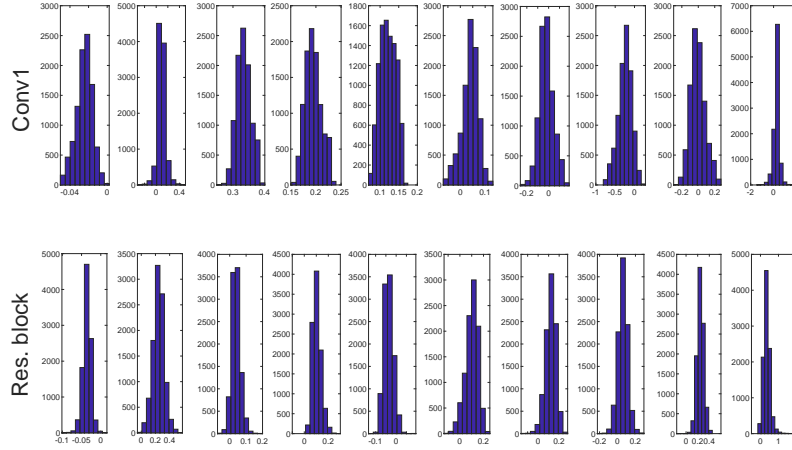
2) *Learned representations can reflect data distribution and quality.* Representation learning is vital to the performance of deep models because learned representations can capture the intrinsic structure of data and provide useful information for the downstream machine learning tasks [16]. In ML research, The value of representations lies in the fact that they characterize the domain and learning task and provide task-specific knowledge [17, 18]. In the context of FL, the similarity of representations are used for refining the model update rules [19, 20], but the distributional difference between representations of heterogeneous data is not yet explored.

Our study is also motivated by a key observation that *representations from neural networks tend*

to have *Gaussian patterns*. As a demonstration we trained two different models (LeNet-5 and ResNet-18) on two different datasets (MNIST and CIFAR-100) separately. Fig. 2a shows the neuron-wise distribution of representations extracted from the first dense layer (FC-1) of LeNet-5. Fig. 2b shows the distribution of fused representations (in a channel-wise manner) extracted from a plain convolution layer and a residual block of ResNet-18.



(a) Representations from FC-1 of a LeNet-5 model after being trained for 1, 6 and 10 epochs on MNIST.



(b) Fused representations from a standard convolution layer (1st row) and a residual block (2nd row) of a ResNet-18 model trained for 100 epochs on CIFAR-100.

Figure 2: (Preliminary experiment) Demonstration of learned representations from a distributional perspective. The representations are generated by forward propagation in model evaluation. Each box corresponds to a randomly sampled element in the representation vector.

These observations motivate us to study the distributional property of data representations and use it as a means to differentiate clients' value.

1.2 Contributions

Our contributions are summarized as follows:

- We first provide theoretical proofs for the observation that data representations from neural nets tend to follow normal distributions, based on which we propose a representation profiling and matching scheme for fast, low-cost representation profile comparison.
- We present a novel FL algorithm FEDPROF that adaptively adjusts clients’ participation probability based on representation profile dissimilarity.
- Results of extensive experiments show that FEDPROF reduces the number of communication rounds by up to 63%, shortens the overall training time (up to $2.4\times$ speedup) while improving the accuracy of the global model by up to 6.8% over FEDAVG and its variants.

2 Related Work

Different from traditional distributed training methods (e.g., [21, 22, 23]), Federated Learning assumes strict constraints of data locality and limited communication capacity [3]. Much effort has been made in optimizing FL and covers a variety of perspectives including communication [3, 24, 25], update rules [26, 27, 28, 29], flexible aggregation [4, 30] and personalization [31, 32, 33].

The control of device participation is imperative in cross-device FL scenarios [34, 35] where the quality of local data is uncontrollable and the clients show varied value for the training task [36]. To this end, the selection of clients is pivotal to the convergence of FL over heterogeneous data and devices [37, 38, 39, 40]. Non-uniform client selection is widely adopted in existing studies [41, 42, 43, 44] and has been theoretically proven with convergence guarantees [43, 5]. Many approaches sample clients based on their performance [37, 45] or aim to jointly optimize the model accuracy and training time [46, 47, 48]. A popular strategy is to use loss as the information to guide client selection [41, 49, 50]. For example, AFL [41] prioritizes the clients with high loss feedback on local data, but it is potentially susceptible to noisy and unexpected data that yield illusive loss values.

Data representations are useful in the context of FL for information exchange [20] or objective adaptation. For example, [19] introduces representation similarities into local objectives. This contrastive learning approach guides local training to avoid model divergence. Nonetheless, the study on the distribution of data representations is still lacking whilst its connection to clients’ training value is hardly explored either.

3 Data Representation Profiling and Matching

In this paper, we consider a typical cross-device FL setting [34], in which multiple end devices collaboratively perform local training on their own datasets $D_i, i = 1, 2, \dots, n$. The server owns a validation dataset D^V for model evaluation.² Every dataset is only accessible to its owner.

Considering the distributional pattern of data representations (Fig. 2) and the role of the global model in FL, we propose to profile the representations of local data using the global model. In this section, we first provide theoretical proofs to support our observation that representations from neural network models tend to follow normal distributions. Then we present a novel scheme to profile data representations and define profile dissimilarity for fast and secure representation comparison.

3.1 Normal Distribution of Representations

In this section we provide theoretical explanations for the Gaussian patterns exhibited by neural networks’ representations. We first make the following definition to facilitate our analysis.

² D^V is usually needed by the server for examining the global model’s quality.

Definition 1 (The Lyapunov’s condition). *A set of random variables $\{Z_1, Z_2, \dots, Z_v\}$ satisfy the Lyapunov’s condition if there exists a δ such that*

$$\lim_{v \rightarrow \infty} \frac{1}{s^{2+\delta}} \sum_{k=1}^v \mathbb{E} [|Z_k - \mu_k|^{2+\delta}] = 0, \quad (1)$$

where $\mu_k = \mathbb{E}[Z_k]$, $\sigma_k^2 = \mathbb{E}[(Z_k - \mu_k)^2]$ and $s = \sqrt{\sum_{k=1}^v \sigma_k^2}$.

The Lyapunov’s condition can be intuitively explained as a limit on the overall variation (with $|Z_k - \mu_k|^{2+\delta}$ being the $(2 + \delta)$ -th moment of Z_k) of a set of random variables.

Now we present Proposition 1 and Proposition 2. The Propositions provide theoretical support for our representation profiling and matching method to be introduced in Section 3.2.

Proposition 1. *The representations from linear operators (e.g., a pre-activation dense layer or a plain convolutional layer) in a neural network tend to follow a normal distribution if the layer’s weighted inputs satisfy the Lyapunov’s condition.*

Proposition 2. *The fused representations³ from non-linear operators (e.g., a hidden layer of LSTM or a residual block of ResNet) in a neural network tend to follow the normal distribution if the layer’s output elements satisfy the Lyapunov’s condition.*

The proofs of Propositions 1 and 2 are provided in Appendices A.1 and A.2, respectively.

We base our proofs on the Lyapunov’s CLT which assumes independence between the variables. The assumption theoretically holds by using the Bayesian network concepts: let X denote the layer’s input and H_k denote the k -th component in its output. The inference through the layer produces dependencies $X \rightarrow H_k$ for all k . According to the *Local Markov Property*, we have H_i independent of any H_j ($j \neq i$) in the same layer given X . Also, the Lyapunov’s condition is typically met when the model is properly initialized and batch normalization is applied. Next, we discuss the proposed representation profiling and matching scheme.

3.2 Distributional Profiling and Matching

Based on the Gaussian pattern of representations, we compress the data representations statistically into a compact form called *representation profiles*. The profile produced by a θ -parameterized global model on a dataset D , denoted by $RP(\theta, D)$, has the following format:

$$RP(\theta, D) = \{\mathcal{N}(\mu_i, \sigma_i^2)\}_{i=1}^q, \quad (2)$$

where q is the profile length determined by the dimensionality of the representations. For example, q is equal to the number of kernels for channel-wise fused representations from a convolutional layer. The tuple (μ_i, σ_i^2) contains the mean and the variance of the i -th representation element.

Local representation profiles are generated by clients and sent to the server for comparison (the cost of transmission is negligible considering each profile is only $q \times 8$ bytes). Let RP_k denote the local profile from client k and RP^B denote the baseline profile (generated in model evaluation) on the server. The dissimilarity between RP_k and RP^B , denoted by $div(RP_k, RP^B)$, is defined as:

$$div(RP_k, RP^B) = \frac{1}{q} \sum_{i=1}^q \text{KL}(\mathcal{N}_i^{(k)} || \mathcal{N}_i^B), \quad (3)$$

where $\text{KL}(\cdot)$ denotes the Kullback–Leibler (KL) divergence. An advantage of our profiling scheme is that a *much simplified* KL divergence formula can be adopted because of the normal distribution

³ *Fused* representations refer to the sum of elements in the original representations produced by a single layer (channel-wise for a residual block).

property (see [51, Appendix B] for details), which yields:

$$\text{KL}(\mathcal{N}_i^{(k)} || \mathcal{N}_i^B) = \log \frac{\sigma_i^B}{\sigma_i^{(k)}} + \frac{(\sigma_i^{(k)})^2 + (\mu_i^{(k)} - \mu_i^B)^2}{2(\sigma_i^B)^2}, \quad (4)$$

Eq. (4) computes the KL divergence without calculating any integral, which is computationally cost-efficient. Besides, the computation of profile dissimilarity can be performed under the Homomorphic Encryption for minimum knowledge disclosure (see Appendix C for details).

4 The Training Algorithm FedProf

Our research aims to optimize the global model over a large group of clients (datasets) of disparate training value. Given the client set $U(|U| = N)$, let D_k denote the local dataset on client k and D^V the validation set on the server. We formulate the optimization problem in (5) where the coefficient ρ_k differentiates the importance of the local objective functions $F_k(\theta)$ and depends on the data in D_k . Our global objective is in a sense similar to the agnostic learning scenario [52] where a non-uniform mixture of local data distributions is implied.

$$\arg \min_{\theta} F(\theta) = \sum_{k=1}^N \rho_k F_k(\theta), \quad (5)$$

where θ denotes the parameters of the global model $h_{\theta} \in \mathcal{H} : \mathcal{X} \rightarrow \mathcal{Y}$ over the feature space \mathcal{X} and target space \mathcal{Y} . The coefficients $\{\rho_k\}_{k=1}^N$ add up to 1. $F_k(\theta)$ is client k 's local objective function of training based on the loss function $\ell(\cdot)$:

$$F_k(\theta) = \frac{1}{|D_k|} \sum_{(x_i, y_i) \in D_k} \ell(h_{\theta}(x_i), y_i), \quad (6)$$

Involving the "right" clients facilitates the convergence. With this motivation we score each client with λ_k each round based on the representation profile dissimilarity:

$$\lambda_k = \exp(-\alpha_k \cdot \text{div}(RP_k, RP^B)), \quad (7)$$

where RP_k and RP^B are generated by an identical global model; α_k is the penalty factor deciding how biased the strategy needs to be against client k . With $\alpha_k = 0$ for all $k = 1, 2, \dots, N$, our strategy is equivalent to random selection. The scores connect the representation profiling and matching scheme to the design of the selective client participation strategy adopted in our FL training algorithm FEDPROF, which is outlined in Algorithm 1 with both client and server processes. The key steps of our algorithm are local representation profiling (line 13), baseline representation profiling (line 18) and client scoring (lines 8 & 9). Fig. 3 illustrates the workflow of the proposed algorithm from representation profiling and matching to scheduling.

The convergence rate of FL algorithms with opportunistic client selection (sampling) has been extensively studied in the literature [5, 43, 4]. Similar to [53, 54, 5], we formally make four assumptions to support our analysis of convergence. Assumptions 1 and 2 are standard in the literature [5, 4, 42] defining the convexity and smoothness properties of the objective functions. Assumptions 3 and 4 bound the variance of the local stochastic gradients and their squared norms in expectation, respectively. These two assumptions are also made in by [5].

Assumption 1. F_1, F_2, \dots, F_N are L -smooth, i.e., for any $k \in U$, x and y : $F_k(y) \leq F_k(x) + (y - x)^T \nabla F_k(x) + \frac{L}{2} \|y - x\|_2^2$

It is obvious that the global objective F is also L -smooth as a linear combination of F_1, F_2, \dots, F_N with $\rho_1, \rho_2, \dots, \rho_N$ being the weights.

Algorithm 1: the FEDPROF protocol

Input : maximum number of rounds T_{max} , local iterations per round τ , client set U , client fraction C , validation set D^V ;
Output: the global model θ

// Server process: running on the server

- 1 Initialize global model θ using a seed
- 2 $v \leftarrow 0$ // version of the latest global model
- 3 Broadcast the seed to all clients for identical model initialization
- 4 Collect initial profiles $\{RP_k\}_{k \in U}$ from all the clients
- 5 $v_k \leftarrow 0, \forall k \in U$
- 6 Generate initial baseline profile $RP^B(0)$ on D^V
- 7 $K \leftarrow |U| \cdot C$
- for** round $T \leftarrow 1$ to T_{max} **do**
- 8 Calculate $div(RP_k(v_k), RP^B(v_k))$ for each client k
- 9 Update client scores $\{\lambda_k\}_{k \in U}$ and compute $\Lambda = \sum_{k \in U} \lambda_k$
- 10 $S \leftarrow$ Choose K clients by probability distribution $\{\frac{\lambda_k}{\Lambda}\}_{k \in U}$
- 11 Distribute θ to the clients in S
- 12 **for** client k in S **in parallel do**
- 13 $v_k \leftarrow v, \forall k \in S$
- 14 $RP_k(v_k) \leftarrow updateProfile(k, \theta, v)$
- 15 $\theta_k \leftarrow localTraining(k, \theta, \tau)$
- 16 **end**
- 17 Collect local profiles from the clients in S
- 18 Update θ via model aggregation
- 19 $v \leftarrow T$
- 20 Evaluate h_θ and generate $RP^B(v)$
- end**
- 21 **return** θ

// Client process: running on client k

updateProfile(k, θ, v):

- 22 Generate RP_k on D_k with the global θ received
- 23 Label profile RP_k with version number v
- 24 Return RP_k

return

localTraining(k, θ, τ):

- 25 $\theta_k \leftarrow \theta$
- 26 **for** step $i \leftarrow 1$ to τ **do**
- 27 Update θ_k using gradient-based method
- 28 **end**
- 29 Return θ_k

return

Assumption 2. F_1, F_2, \dots, F_N are μ -strongly convex, i.e., for all $k \in U$ and any x, y : $F_k(y) \geq F_k(x) + (y - x)^T \nabla F_k(x) + \frac{\mu}{2} \|y - x\|_2^2$

Assumption 3. The variance of local stochastic gradients on each device is bounded: For all $k \in U$, $E\|\nabla F_k(\theta_k(t), \xi_{t,k}) - F_k(\theta_k(t))\|^2 \leq \epsilon^2$

Assumption 4. The squared norm of local stochastic gradients on each device is bounded: For all $k \in U$, $E\|\nabla F_k(\theta_k(t), \xi_{t,k})\|^2 \leq G^2$

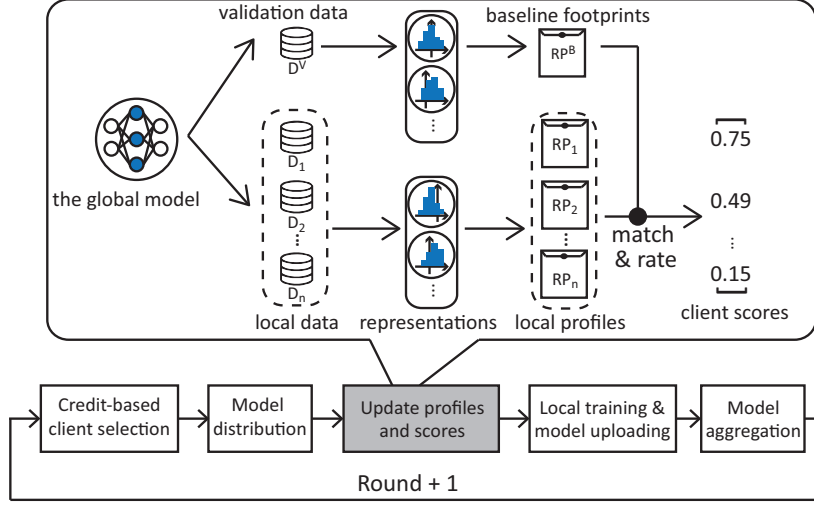


Figure 3: The workflow of the proposed FEDPROF algorithm.

Inspired by these studies, we present Theorem 1 to guarantee the global model’s convergence for our algorithm.

Theorem 1. *Using partial aggregation and our selection strategy that satisfies $\alpha_k = -\frac{\ln(\Delta\rho_k)}{\text{div}(\text{RP}_k, \text{RP}^B)}$, the global model $\theta(t)$ converges in expectation given an aggregation interval $\tau \geq 1$ and a decreasing step size (learning rate) $\eta_t = \frac{2}{\mu(t+\gamma)}$.*

$$\mathbb{E}[F(\theta(t))] - F^* \leq \frac{L}{(\gamma + t)} \left(\frac{2(\mathcal{B} + \mathcal{C})}{\mu^2} + \frac{\gamma + 1}{2} \Delta_1 \right), \quad (8)$$

where $t \in T_A = \{n\tau | n = 1, 2, \dots\}$, $\gamma = \max\{\frac{8L}{\mu}, \tau\} - 1$, $\mathcal{B} = \sum_{k=1}^N \rho_k^2 \epsilon_k^2 + 6L\Gamma + 8(\tau - 1)^2 G^2$, $\mathcal{C} = \frac{4}{K} \tau^2 G^2$, $\Gamma = F^* - \sum_{k=1}^N \rho_k F_k^*$, $\Delta_1 = \mathbb{E}\|\bar{\theta}(1) - \theta^*\|^2$, $\Lambda = \sum_{k=1}^N \lambda_k$, and $K = |S(t)| = N \cdot C$.

The proof of Theorem 1 is provided in Appendix B where the basic assumptions and the supporting lemmas are also formally presented.

5 Experiments

We conducted extensive experiments to evaluate FEDPROF under various FL settings. Apart from FEDAVG [2] as the baseline, we also reproduced several state-of-the-art FL algorithms for comparison. These include CFCFM [30], FEDAVG-RP [5], FEDPROX [26], FEDADAM [28] and AFL [55]. For fair comparison, the algorithms are grouped by the aggregation method (i.e., full aggregation and partial aggregation) and configured based on the parameter settings suggested in their papers. Note that our algorithm can adapt to both aggregation methods.

5.1 Experimental Setup

We built a discrete event-driven, simulation-based FL system and implemented the training logic under the Pytorch framework (Build 1.7.0). To evaluate the algorithms in disparate FL scenarios, we set up three different tasks using three public datasets: *GasTurbine* (from the UCI repository⁴), *EMNIST* and *CIFAR-10*. With *GasTurbine* the goal is to learn a carbon monoxide (CO) and nitrogen oxides

⁴<https://archive.ics.uci.edu/ml/datasets.php>

Table 1: The implemented FL algorithms for comparison

Algorithm	Aggregation method	Rule of selection
FEDAVG [2]	full aggregation	random selection
CFCFM [30]	full aggregation	submission order
FEDAVG-RP [5]	partial (Scheme II)	random selection
FEDPROX [26]	partial aggregation	weighted random by data ratio
FEDADAM [28]	partial with momentum	random selection
AFL [41]	partial with momentum	local loss valuation
FEDPROF (ours)	full/partial aggregation	weighted random by score

(NOx) emission prediction model over a network of 50 sensors. Using EMNIST and CIFAR-10 we set up two image classification tasks with different models (LeNet-5 [56] for EMNIST and ShuffleNet v2 [57] for CIFAR-10). We also differentiate the system scale—500 mobile clients for EMNIST and 10 dataholders for CIFAR-10—to emulate cross-device and cross-silo scenarios [34] respectively. The penalty factors α are set to (a, a, \dots, a) where $a=10.0$, 10.0 and 25.0 for GasTurbine, EMNIST and CIFAR-10, respectively.

In all the tasks, data sharing is not allowed between any parties and the data are non-IID across the clients. We made local data statistically heterogeneous by forcing class imbalance (for CIFAR and EMNIST)⁵ or size imbalance (for GasTurbine).⁶ We introduce a diversity of noise into the local datasets to simulate the discrepancy in data quality: for GasTurbine, 50% of the sensors produce noisy data (including 10% polluted); for EMNIST and CIFAR-10, a certain percentage of local datasets are irrelevant images or low-quality images (blurred or affected by salt-and-pepper noise). Aside from data heterogeneity, all the clients are also heterogeneous in performance and communication bandwidth. Considering the client population and based on the scale of the training participants suggested by [34], the selection fraction C is set to 0.2, 0.05 and 0.5 for the three tasks, respectively. More experimental settings are listed in Table 2.

Table 2: Experimental setup.

Setting	Symbol	Task 1	Task 2	Task 3
Model	h_θ	MLP	LeNet-5	ShuffleNet v2
Dataset	D	GasTurbine	EMNIST digits	CIFAR-10
Total data size	$ D $	36.7k	280k	60k
Validation set size	$ D^V $	11.0k	40k	10k
Client population	N	50	500	10
Data distribution	-	$\mathcal{N}(514, 101^2)$	non-IID, dc \approx 60%	non-IID, dc $>$ 30%
Noise applied	-	pollution, Gaussian noise	fake, blur, pixel	fake, blur, pixel
Client specification (GHz)	s_k	$\mathcal{N}(0.5, 0.1^2)$	$\mathcal{N}(1.0, 0.2^2)$	$\mathcal{N}(3.0, 0.4^2)$
Comm. bandwidth (MHz)	bw_k	$\mathcal{N}(0.7, 0.1^2)$	$\mathcal{N}(1.0, 0.3^2)$	$\mathcal{N}(2.0, 0.2^2)$
Signal-to-noise ratio	SNR	7 dB	10 dB	10 dB
Bits per sample	BPS	11*8*4	28*28*1*8	32*32*3*8
Cycles per bit	CPB	300	400	400
# of local epochs	E	2	5	6
Batch size	-	8, 32	32, 128	16, 32
Loss function	ℓ	MSE	NLL	CE
Learning rate	η	5e-3	5e-3	1e-2
learning rate decay	-	0.994	0.99	0.999

⁵Each client has a dominant class that accounts for roughly 60% (for EMNIST) or 37% (for CIFAR) of the local data size.

⁶The sizes of local datasets follow a normal distribution

For GasTurbine, the total population is 50 and the data collected by a proportion of the sensors (i.e., end devices of this task) are of low-quality: 10% of the sensors are polluted (with features taking invalid values) and 40% of them produce noisy data. For EMNIST, we set up a relatively large population (500 end devices) and spread the data (from the *digits* subset) across the devices with strong class imbalance—roughly 60% of the samples on each device fall into the same class. Besides, many local datasets are of low-quality: the images on 15% of the clients are irrelevant (valueless for the training of this task), 20% are (Gaussian) blurred, and 25% are affected by the salt-and-pepper noise (random black and white dots on the image, density=0.3). For CIFAR-10, same types of noise are applied but with lower percentages (10%, 20% and 20%) of clients affected. The class imbalance degree in local data distribution for the 10 clients is set to 37%, i.e., each local dataset is dominated by a single class that accounts for approximately 37% of the total size.

A sufficiently long running time is guarantee for all the three FL tasks. The maximum number of rounds T_{max} is set to 500 for the GasTurbine task. For EMNIST, T_{max} is set to 240 for the full aggregation and 80 for partial aggregation respectively considering their discrepancy in convergence speed. For CIFAR-10, T_{max} is set to 150 for the full aggregation and 120 for partial aggregation respectively, which are adequate for the global model to converge in our settings.

In each FL round, the server selects a fraction (i.e., C) of clients, distributes the global model to these clients and waits for them to finish the local training and upload the models. Given a selected set of clients S , the time cost and energy cost of a communication round can be formulated as:

$$T_{round} = \max_{k \in S} \{T_k^{comm} + T_k^{train} + T_k^{RP}\}, \quad (9)$$

$$E_k = E_k^{comm} + E_k^{train} + E_k^{RP}. \quad (10)$$

where T_k^{comm} and T_k^{train} are the communication time and local training time, respectively. The device-side energy consumption E_k mainly comes from model transmission (through wireless channels) and local processing (training), corresponding to E_k^{comm} and E_k^{train} , respectively. T_k^{RP} and E_k^{RP} estimate the time and energy costs for generating and uploading local profiles and only apply to FEDPROF.

Eq. (9) formulates the length of one communication round of FL, where T_k^{comm} can be modeled by Eq. (11) according to [63], where bw_k is the downlink bandwidth of device k (in MHz); SNR is the Signal-to-Noise Ratio of the communication channel, which is set to be constant as in general the end devices are coordinated by the base stations for balanced SNR with the fairness-based policies; m_{size} is the size (in MB) of the (encrypted) model; the model upload time is twice as much as that for model download since the uplink bandwidth is set to 50% of the downlink bandwidth.

$$\begin{aligned} T_k^{comm} &= T_k^{upload} + T_k^{download} \\ &= 2 \times T_k^{download} + T_k^{download} \\ &= 3 \times \frac{m_{size}}{bw_k \cdot \log(1 + SNR)}, \end{aligned} \quad (11)$$

T_k^{train} in Eq. (9) can be modeled by Eq. (12), where s_k is the device performance (in GHz) and the numerator computes the total number of processor cycles required for processing E epochs of local training on D_k .

$$T_k^{train} = \frac{E \cdot |D_k| \cdot BPS \cdot CPB}{s_k}, \quad (12)$$

T_k^{RP} consists of two parts: T_k^{RPgen} for local model evaluation (to generate the profiles of D_k) and T_k^{RPup} for uploading the profile. T_k^{RP} can be modeled as:

$$\begin{aligned}
T_k^{RP} &= T_k^{RPgen} + T_k^{RPup} \\
&= \frac{1}{E} T_k^{train} + \frac{RPsize}{\frac{1}{2}bw_k \cdot \log(1 + SNR)},
\end{aligned} \tag{13}$$

where T_k^{RPgen} is estimated as the time cost of one epoch of local training; T_k^{RPup} is computed in a similar way to the calculation of T_k^{comm} in Eq. (11) (where the uplink bandwidth is set as one half of the total bw_k); $RPsize$ is the size of a profile, which is equal to $4 \times 2 \times q = 8 \times q$ (four bytes for each floating point number) according to our definition of profile in (2).

Using Eq. (10) we model the energy cost of each end device by mainly considering the energy consumption of the transmitters for communication (Eq. 14) and on-device computation for local training (Eq. 15). For FEDPROF, there is an extra energy cost for generating and uploading profiles (Eq. 16).

$$E_k^{comm} = P_{trans} \cdot T_k^{comm} \tag{14}$$

$$E_k^{train} = P_f s_k^3 \cdot T_k^{train} \tag{15}$$

$$E_k^{RP} = P_{trans} \cdot T_k^{RPup} + P_f s_k^3 \cdot T_k^{RPgen}, \tag{16}$$

where $P_f s_k^3$ is a simplified computation power consumption model [64] and P_f is the power of a baseline processor. P_{trans} is the transmitter's power. We set P_{trans} and P_f to 0.75 W and 0.7 W respectively based on the benchmarking data provided by [65] and [66].

5.2 Empirical Results

We evaluated the performance of our FEDPROF algorithm in terms of the efficacy (i.e., best accuracy achieved) and efficiency (i.e., costs for convergence) in establishing a global model for the three tasks. Tables 3, 4 and 5 report the averaged results (including best accuracy achieved and convergence costs given a preset accuracy goal) of multiple runs with standard deviations. Figs. 4 and 5 plot the accuracy traces from the round-wise evaluations of the global model for the full and partial aggregation groups, respectively.

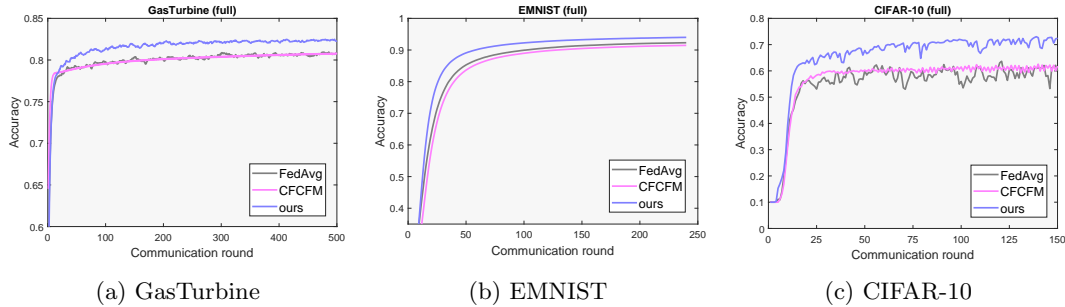


Figure 4: The traces of the global model’s evaluation accuracy by running FL with algorithms in the full aggregation group.

1) *Convergence in different aggregation modes:* Our results show a great difference in convergence rate under different aggregation modes. From Figs. 4 and 5, we observe that partial aggregation facilitates faster convergence of the global model than full aggregation, which is consistent with the observations made by [5]. The advantage is especially obvious on EMNIST where FEDAVG-RP

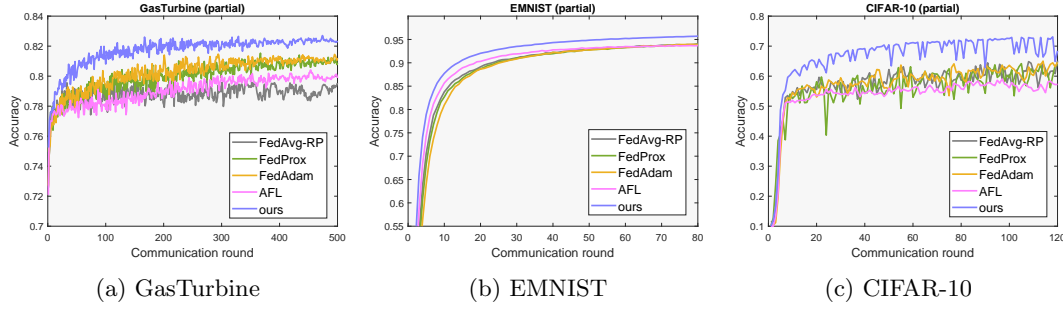


Figure 5: The traces of the global model’s evaluation accuracy by running FL with algorithms in the partial aggregation group.

Table 3: Summary of the evaluation results on *GasTurbine*. The best accuracy is achieved by running for long enough. Other metrics are recorded upon the global model reaching 80% accuracy. Standard deviations of multiple runs are shown after the \pm symbol.

GasTurbine (full aggregation)				
	Best accuracy	For accuracy@0.8		
		Rounds needed	Time (minutes)	Energy (Wh)
FEDAVG	0.817 ± 0.005	82+-73	47.7+-42.3	4.59+-4.11
CFCFM	0.809 ± 0.006	167+-147	68.9+-60.8	8.15+-7.17
Ours	0.832 ± 0.005	38±23	22.3±13.7	2.15±1.29
GasTurbine (partial aggregation)				
FEDAVG-RP	0.820 ± 0.007	28±11	16.8±7.1	1.62±0.68
FEDPROX	0.829 ± 0.003	35±19	20.3±11.4	1.78±0.98
FEDADAM	0.828 ± 0.006	46±35	27.2±21.2	2.59±1.98
AFL	0.818 ± 0.003	54±51	30.2±27.1	2.99±2.81
Ours	0.838 ± 0.005	19±9	11.0±5.5	1.07±0.53

requires <30 communication rounds to reach the 90% accuracy whilst the standard FEDAVG needs 100+. On all three tasks, our FEDPROF algorithm significantly improves the convergence speed in both groups of comparison especially for the full aggregation mode.

2) *Best accuracy of the global model*: Throughout the FL training process, the global model is evaluated each round on the server who keeps track of the best accuracy achieved. As shown in the 2nd column of Tables 3, 4 and 5, our FEDPROF algorithm achieves up to 1.8%, 1.7% and 6.8% accuracy improvement over the baselines FEDAVG and FEDAVG-RP on GasTurbine, EMNIST and CIFAR-10, respectively.

3) *Total communication rounds for convergence*: The number of communication rounds required for reaching convergence is a key efficiency indicator. On GasTurbine, our algorithm takes *less than half* the communication rounds required by other algorithms in most cases. On EMNIST, our algorithm reaches 90% accuracy within 60 rounds whilst FEDAVG and CFCFM need more than 100 with full aggregation. AFL adopts a loss-oriented client selection strategy, which shows the closest performance to our algorithm on EMNIST but fails to reach the 60% accuracy mark on CIFAR-10. A possible explanation is that noisy data (with higher losses) are less harmful at early training stage but will mislead the model update to local optima.

4) *Total time needed for convergence*: The overall time consumption is closely related to total communication rounds needed for convergence and the time cost for each round. Algorithms requiring more rounds to converge typically take longer to reach the accuracy target except the case of CFCFM, which priorities the clients that work faster. By contrast, our algorithm accelerates convergence

Table 4: Summary of the evaluation results on *EMNIST*. Stats (except for 'Best accuracy') are recorded with a 90% accuracy goal.

EMNIST (full aggregation)				
	Best accuracy	For accuracy@0.9		
		Rounds needed	Time (minutes)	Energy (Wh)
FEDAVG	0.923±0.004	103±13	115.8±16.2	15.83±2.04
CFCFM	0.918±0.008	136±42	46.2±14.5	15.02±4.59
Ours	0.940±0.004	59±5	67.1±12.4	9.49±0.66
EMNIST (partial aggregation)				
FEDAVG-RP	0.941±0.003	23±3	26.5±4.3	3.60±0.37
FEDPROX	0.941±0.005	23±3	27.7±6.8	3.69±0.70
FEDADAM	0.941±0.003	26±3	29.1±4.3	3.99±0.47
AFL	0.939±0.005	19±4	22.4±6.8	2.93±0.57
Ours	0.957±0.003	15±1	16.1±3.3	2.43±0.25

Table 5: Summary of the evaluation results on *CIFAR-10*. Stats (except for 'Best accuracy') are recorded with a 60% accuracy goal.

CIFAR (full aggregation)				
	Best accuracy	For accuracy@0.6		
		Rounds needed	Time (minutes)	Energy (Wh)
FEDAVG	0.665±0.011	38±10	91.4±26.3	93.52±17.14
CFCFM	0.638±0.008	32±5	74.0±8.7	79.90±15.18
Ours	0.733±0.003	14±1	38.8±3.7	39.67±1.14
CIFAR (partial aggregation)				
FEDAVG-RP	0.674±0.004	24±2	56.7±3.5	59.73±9.88
FEDPROX	0.682±0.009	28±6	66.2±17.8	56.85±7.76
FEDADAM	0.669±0.014	28±2	68.5±4.9	68.96±5.10
AFL	0.599±0.007	-	-	-
Ours	0.735±0.007	9±1	23.5±1.29	24.54±1.11

by addressing the heterogeneity of data and data quality, providing a $2.1\times$ speedup over FEDAVG on GasTurbine and $2.4\times$ speedup over FEDAVG-RP on CIFAR-10. Our strategy also has a clear advantage over CFCFM, FEDPROX, FEDADAM and AFL for all three tasks, yielding a significant reduction (up to 65.7%) in the wall-clock time consumption until convergence.

5) *Energy consumption of end devices*: A main concern for the end devices, as the participants of FL, is their power usage (in training and communications). Full aggregation methods experience slower convergence and thus endure higher energy cost on the devices. For example, with a small selection fraction ($C=0.05$) and a large scale ($N=500$) for the EMNIST task, FEDAVG and CFCFM consume over 15 Wh to reach the target accuracy, in which case our algorithm reduces the energy cost by over 37%. Under the CIFAR-10 FL setting with partial aggregation, the reduction by our algorithm reaches 58.9% and 64.4%—saving over 35 Wh—as compared to FEDAVG-RP and FEDADAM, respectively.

6) *Differentiated participation with FEDPROF*: In figs. 6 and 7 we visualize the behaviour of our selection strategy on the three tasks. Fig. 6 shows how many times clients get selected under the GasTurbine and EMNIST settings. We can observe that the clients with polluted samples or noisy data are significantly less involved in training the prediction model for GasTurbine. On EMNIST, our algorithm also effectively limits (basically excludes) the clients who hold image data of poor quality (i.e., irrelevant or severely blurred), whereas the clients with moderately noisy images are selected with reduced frequency as compared to those with normal data. Fig. 7 reveals the *distribution of clients' scores* assigned by FEDPROF throughout the training process on CIFAR-10, where our strategy

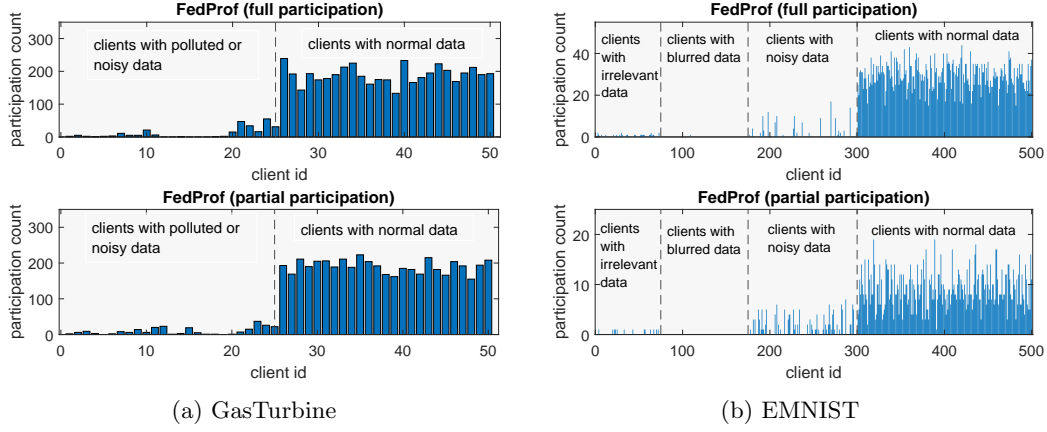


Figure 6: Total counts by client of participation (i.e., being selected) on the GasTurbine and EMNIST tasks with our strategy. For clarity, clients are indexed according to their local data quality.

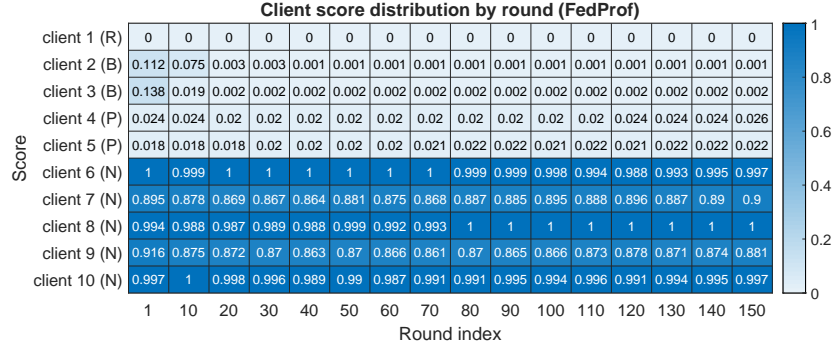


Figure 7: A heatmap illustrating the dynamic distribution of clients' scores (normalized) for FEDPROF on CIFAR-10. The annotations 'R', 'B' or 'P' indicate the possession of image data that are irrelevant, blurred or affected by pixel-level noises whilst 'N' means that of normal data.

effectively avoids the low-value clients since the initial round, demonstrating that our distributional representation profiling and matching method can provide strong evidence of local data's quality and informativeness. A potential issue of having the preference towards some of the devices is about fairness. Nonetheless, one can apply our algorithm together with an incentive mechanism (e.g., [58]) to address it.

6 Conclusion

Federated learning provides a privacy-preserving approach to decentralized training but is vulnerable to the heterogeneity and uncertain quality of on-device data. In this paper, we use a novel approach to address the issue without violating the data locality restriction. We first provide key insights for the distribution of data representations and then develop a dynamic data representation profiling and matching scheme. Based on the scheme we propose a selective FL training algorithm FEDPROF that adaptively adjusts clients' participation chance based on their profile dissimilarity. We have conducted extensive experiments on public datasets under various FL settings. Evaluation results show that our algorithm significantly improves the efficiency of FL and the global model's accuracy whilst reducing the time and energy costs for the global model to converge. Our future study may involve extending

our selective strategy to other variants of FL scenarios such as personalized FL, vertical FL and federated ensemble learning.

References

- [1] Robert van der Meulen. What edge computing means for infrastructure and operations leaders. <https://www.gartner.com/smarterwithgartner/what-edge-computing-means-for-infrastructure-and-operations-leaders/>, 2018. Accessed: 2021-07-10.
- [2] Brendan McMahan, Eider Moore, Daniel Ramage, Seth Hampson, and Blaise Agüera y Arcas. Communication-efficient learning of deep networks from decentralized data. In *Artificial Intelligence and Statistics (AISTATS)*, pages 1273–1282. PMLR, 2017.
- [3] Jakub Konečný, H Brendan McMahan, Felix X Yu, Peter Richtárik, Ananda Theertha Suresh, and Dave Bacon. Federated learning: Strategies for improving communication efficiency. *arXiv preprint arXiv:1610.05492*, 2016.
- [4] Shiqiang Wang, Tiffany Tuor, Theodoros Salonidis, Kin K Leung, Christian Makaya, Ting He, and Kevin Chan. Adaptive federated learning in resource constrained edge computing systems. *IEEE Journal on Selected Areas in Communications*, 37(6):1205–1221, 2019.
- [5] Xiang Li, Kaixuan Huang, Wenhao Yang, Shusen Wang, and Zhihua Zhang. On the convergence of fedavg on non-iid data. In *International Conference on Learning Representations*, 2019.
- [6] Andrew Hard, Kanishka Rao, Rajiv Mathews, Swaroop Ramaswamy, Françoise Beaufays, Sean Augenstein, Hubert Eichner, Chloé Kiddon, and Daniel Ramage. Federated learning for mobile keyboard prediction. *arXiv preprint arXiv:1811.03604*, 2018.
- [7] Arjun Nitin Bhagoji, Supriyo Chakraborty, Prateek Mittal, and Seraphin Calo. Analyzing federated learning through an adversarial lens. In *International Conference on Machine Learning*, pages 634–643. PMLR, 2019.
- [8] Eugene Bagdasaryan, Andreas Veit, Yiqing Hua, Deborah Estrin, and Vitaly Shmatikov. How to backdoor federated learning. In *International Conference on Artificial Intelligence and Statistics*, pages 2938–2948. PMLR, 2020.
- [9] Minghong Fang, Xiaoyu Cao, Jinyuan Jia, and Neil Gong. Local model poisoning attacks to byzantine-robust federated learning. In *29th USENIX Security Symposium (USENIX Security 20)*, pages 1605–1622, 2020.
- [10] Vale Tolpegin, Stacey Truex, Mehmet Emre Gursoy, and Ling Liu. Data poisoning attacks against federated learning systems. In *European Symposium on Research in Computer Security*, pages 480–501. Springer, 2020.
- [11] Jaejun Yoo, Namhyuk Ahn, and Kyung-Ah Sohn. Rethinking data augmentation for image super-resolution: A comprehensive analysis and a new strategy. In *Proceedings of the IEEE/CVF Conference on Computer Vision and Pattern Recognition*, pages 8375–8384, 2020.
- [12] Wei-Chao Lin, Chih-Fong Tsai, Ya-Han Hu, and Jing-Shang Jhang. Clustering-based undersampling in class-imbalanced data. *Information Sciences*, 409:17–26, 2017.
- [13] Yin Cui, Menglin Jia, Tsung-Yi Lin, Yang Song, and Serge Belongie. Class-balanced loss based on effective number of samples. In *Proceedings of the IEEE/CVF conference on computer vision and pattern recognition*, pages 9268–9277, 2019.

- [14] Da Yu, Huishuai Zhang, Wei Chen, Jian Yin, and Tie-Yan Liu. How does data augmentation affect privacy in machine learning? In *Proceedings of the AAAI Conference on Artificial Intelligence*, volume 35, pages 10746–10753, 2021.
- [15] AJ Feelders. Learning from biased data using mixture models. In *KDD*, pages 102–107, 1996.
- [16] Yoshua Bengio, Aaron Courville, and Pascal Vincent. Representation learning: A review and new perspectives. *IEEE transactions on pattern analysis and machine intelligence*, 35(8):1798–1828, 2013.
- [17] Ari S Morcos, Maithra Raghu, and Samy Bengio. Insights on representational similarity in neural networks with canonical correlation. In *Proceedings of the 32nd International Conference on Neural Information Processing Systems*, pages 5732–5741, 2018.
- [18] Simon Kornblith, Mohammad Norouzi, Honglak Lee, and Geoffrey Hinton. Similarity of neural network representations revisited. In *International Conference on Machine Learning*, pages 3519–3529. PMLR, 2019.
- [19] Qinbin Li, Bingsheng He, and Dawn Song. Model-contrastive federated learning. In *Proceedings of the IEEE/CVF Conference on Computer Vision and Pattern Recognition*, pages 10713–10722, 2021.
- [20] Siwei Feng and Han Yu. Multi-participant multi-class vertical federated learning. *arXiv preprint arXiv:2001.11154*, 2020.
- [21] Dan Alistarh, Demjan Grubic, Jerry Li, Ryota Tomioka, and Milan Vojnovic. Qsgd: Communication-efficient sgd via gradient quantization and encoding. *Advances in Neural Information Processing Systems*, 30:1709–1720, 2017.
- [22] Jiaxiang Wu, Weidong Huang, Junzhou Huang, and Tong Zhang. Error compensated quantized sgd and its applications to large-scale distributed optimization. In *International Conference on Machine Learning*, pages 5325–5333. PMLR, 2018.
- [23] Shuxin Zheng, Qi Meng, Taifeng Wang, Wei Chen, Nenghai Yu, Zhi-Ming Ma, and Tie-Yan Liu. Asynchronous stochastic gradient descent with delay compensation. In *International Conference on Machine Learning*, pages 4120–4129. PMLR, 2017.
- [24] Solmaz Niknam, Harpreet S Dhillon, and Jeffrey H Reed. Federated learning for wireless communications: Motivation, opportunities, and challenges. *IEEE Communications Magazine*, 58(6):46–51, 2020.
- [25] Laizhong Cui, Xiaoxin Su, Yipeng Zhou, and Yi Pan. Slashing communication traffic in federated learning by transmitting clustered model updates. *IEEE Journal on Selected Areas in Communications*, 2021.
- [26] Tian Li, Anit Kumar Sahu, Manzil Zaheer, Maziar Sanjabi, Ameet Talwalkar, and Virginia Smith. Federated optimization in heterogeneous networks. In *The 3rd MLSys Conference*, 2020.
- [27] Wentai Wu, Ligang He, Weiwei Lin, and Rui Mao. Accelerating federated learning over reliability-agnostic clients in mobile edge computing systems. *IEEE Transactions on Parallel and Distributed Systems*, 32(7):1539–1551, 2021.
- [28] David Leroy, Alice Coucke, Thibaut Lavril, Thibault Gisselbrecht, and Joseph Dureau. Federated learning for keyword spotting. In *ICASSP 2019-2019 IEEE International Conference on Acoustics, Speech and Signal Processing (ICASSP)*, pages 6341–6345. IEEE, 2019.

- [29] WANG Luping, WANG Wei, and LI Bo. Cmf1: Mitigating communication overhead for federated learning. In *2019 IEEE 39th International Conference on Distributed Computing Systems (ICDCS)*, pages 954–964. IEEE, 2019.
- [30] Wentai Wu, Ligang He, Weiwei Lin, Rui Mao, Carsten Maple, and Stephen A Jarvis. Safa: a semi-asynchronous protocol for fast federated learning with low overhead. *IEEE Transactions on Computers*, 70(5):655–668, 2021.
- [31] Alireza Fallah, Aryan Mokhtari, and Asuman Ozdaglar. Personalized federated learning with theoretical guarantees: A model-agnostic meta-learning approach. *Advances in Neural Information Processing Systems*, 33:3557–3568, 2020.
- [32] Alysia Ziying Tan, Han Yu, Lizhen Cui, and Qiang Yang. Towards personalized federated learning. *arXiv preprint arXiv:2103.00710*, 2021.
- [33] Yuyang Deng, Mohammad Mahdi Kamani, and Mehrdad Mahdavi. Adaptive personalized federated learning. *arXiv preprint arXiv:2003.13461*, 2020.
- [34] Peter Kairouz, H Brendan McMahan, Brendan Avent, Aurélien Bellet, Mehdi Bennis, Arjun Nitin Bhagoji, Kallista Bonawitz, Zachary Charles, Graham Cormode, Rachel Cummings, et al. Advances and open problems in federated learning. *arXiv preprint arXiv:1912.04977*, 2019.
- [35] Haibo Yang, Minghong Fang, and Jia Liu. Achieving linear speedup with partial worker participation in non-iid federated learning. In *International Conference on Learning Representations*, 2020.
- [36] Tiffany Tuor, Shiqiang Wang, Bong Jun Ko, Changchang Liu, and Kin K. Leung. Overcoming noisy and irrelevant data in federated learning. *arXiv preprint arXiv:2001.08300*, 2020.
- [37] Takayuki Nishio and Ryo Yonetani. Client selection for federated learning with heterogeneous resources in mobile edge. In *ICC 2019-2019 IEEE International Conference on Communications (ICC)*, pages 1–7. IEEE, 2019.
- [38] Jianyu Wang, Qinghua Liu, Hao Liang, Gauri Joshi, and H Vincent Poor. Tackling the objective inconsistency problem in heterogeneous federated optimization. *arXiv preprint arXiv:2007.07481*, 2020.
- [39] Zheng Chai, Hannan Fayyaz, Zeshan Fayyaz, Ali Anwar, Yi Zhou, Nathalie Baracaldo, Heiko Ludwig, and Yue Cheng. Towards taming the resource and data heterogeneity in federated learning. In *2019 USENIX Conference on Operational Machine Learning (OpML 19)*, pages 19–21, 2019.
- [40] Durmus Alp Emre Acar, Yue Zhao, Ramon Matas, Matthew Mattina, Paul Whatmough, and Venkatesh Saligrama. Federated learning based on dynamic regularization. In *International Conference on Learning Representations*, 2020.
- [41] Jack Goetz, Kshitiz Malik, Duc Bui, Seungwhan Moon, Honglei Liu, and Anuj Kumar. Active federated learning. *arXiv preprint arXiv:1909.12641*, 2019.
- [42] Yae Jee Cho, Jianyu Wang, and Gauri Joshi. Client selection in federated learning: Convergence analysis and power-of-choice selection strategies. *arXiv preprint arXiv:2010.01243*, 2020.
- [43] Wenlin Chen, Samuel Horvath, and Peter Richtarik. Optimal client sampling for federated learning. *arXiv preprint arXiv:2010.13723*, 2020.
- [44] Hao Wang, Zakhary Kaplan, Di Niu, and Baochun Li. Optimizing federated learning on non-iid data with reinforcement learning. In *IEEE INFOCOM 2020-IEEE Conference on Computer Communications*, pages 1698–1707. IEEE, 2020.

- [45] Zheng Chai, Ahsan Ali, Syed Zawad, Stacey Truex, Ali Anwar, Nathalie Baracaldo, Yi Zhou, Heiko Ludwig, Feng Yan, and Yue Cheng. Tifl: A tier-based federated learning system. In *Proceedings of the 29th International Symposium on High-Performance Parallel and Distributed Computing*, pages 125–136, 2020.
- [46] Wenqi Shi, Sheng Zhou, and Zhisheng Niu. Device scheduling with fast convergence for wireless federated learning. In *ICC 2020-2020 IEEE International Conference on Communications (ICC)*, pages 1–6. IEEE, 2020.
- [47] Mingzhe Chen, H Vincent Poor, Walid Saad, and Shuguang Cui. Convergence time optimization for federated learning over wireless networks. *IEEE Transactions on Wireless Communications*, 20(4):2457–2471, 2020.
- [48] Mingzhe Chen, Nir Shlezinger, H Vincent Poor, Yonina C Eldar, and Shuguang Cui. Communication-efficient federated learning. *Proceedings of the National Academy of Sciences*, 118(17), 2021.
- [49] Fan Lai, Xiangfeng Zhu, Harsha V Madhyastha, and Mosharaf Chowdhury. Oort: Efficient federated learning via guided participant selection. In *15th USENIX Symposium on Operating Systems Design and Implementation (OSDI 21)*, pages 19–35, 2021.
- [50] Dipankar Sarkar, Ankur Narang, and Sumit Rai. Fed-focal loss for imbalanced data classification in federated learning. *arXiv preprint arXiv:2011.06283*, 2020.
- [51] Stephen J Roberts and Will D Penny. Variational bayes for generalized autoregressive models. *IEEE Transactions on Signal Processing*, 50(9):2245–2257, 2002.
- [52] Mehryar Mohri, Gary Sivek, and Ananda Theertha Suresh. Agnostic federated learning. In *International Conference on Machine Learning*, pages 4615–4625. PMLR, 2019.
- [53] Sebastian U Stich, Jean-Baptiste Cordonnier, and Martin Jaggi. Sparsified sgd with memory. *Advances in Neural Information Processing Systems*, 31:4447–4458, 2018.
- [54] Yuchen Zhang, John C Duchi, and Martin J Wainwright. Communication-efficient algorithms for statistical optimization. *The Journal of Machine Learning Research*, 14(1):3321–3363, 2013.
- [55] Jonathan Goetz. *Active Learning in Non-parametric and Federated Settings*. PhD thesis, University of Michigan, 2020.
- [56] Yann LeCun, Léon Bottou, Yoshua Bengio, and Patrick Haffner. Gradient-based learning applied to document recognition. *Proceedings of the IEEE*, 86(11):2278–2324, 1998.
- [57] Ningning Ma, Xiangyu Zhang, Hai-Tao Zheng, and Jian Sun. Shufflenet v2: Practical guidelines for efficient cnn architecture design. In *Proceedings of the European conference on computer vision (ECCV)*, pages 116–131, 2018.
- [58] Han Yu, Zelei Liu, Yang Liu, Tianjian Chen, Mingshu Cong, Xi Weng, Dusit Niyato, and Qiang Yang. A fairness-aware incentive scheme for federated learning. In *Proceedings of the AAAI/ACM Conference on AI, Ethics, and Society*, pages 393–399, 2020.
- [59] Don S Lemons. *An Introduction to Stochastic Processes in Physics*. Johns Hopkins University Press, 2003.
- [60] Patrick Billingsley. *Probability and measure*. John Wiley & Sons, 2008.
- [61] Kaiming He, Xiangyu Zhang, Shaoqing Ren, and Jian Sun. Deep residual learning for image recognition. In *Proceedings of the IEEE conference on computer vision and pattern recognition*, pages 770–778, 2016.

- [62] Craig Gentry. Fully homomorphic encryption using ideal lattices. In *Proceedings of the forty-first annual ACM symposium on Theory of computing*, pages 169–178, 2009.
- [63] Nguyen H Tran, Wei Bao, Albert Zomaya, Minh NH Nguyen, and Choong Seon Hong. Federated learning over wireless networks: Optimization model design and analysis. In *IEEE INFOCOM 2019-IEEE Conference on Computer Communications*, pages 1387–1395. IEEE, 2019.
- [64] Jie Song, Tiantian Li, Zhi Wang, and Zhiliang Zhu. Study on energy-consumption regularities of cloud computing systems by a novel evaluation model. *Computing*, 95(4):269–287, 2013.
- [65] Aaron Carroll, Gernot Heiser, et al. An analysis of power consumption in a smartphone. In *USENIX annual technical conference*, volume 14, pages 21–21. Boston, MA, 2010.
- [66] Pijush Kanti Dutta Pramanik, Nilanjan Sinhababu, Bulbul Mukherjee, Sanjeevikumar Padmanaban, Aranyak Maity, Bijoy Kumar Upadhyaya, Jens Bo Holm-Nielsen, and Prasenjit Choudhury. Power consumption analysis, measurement, management, and issues: A state-of-the-art review of smartphone battery and energy usage. *IEEE Access*, 7:182113–182172, 2019.

A Proof of Propositions

A.1 Proof of Proposition 1

Without loss of generality, we provide the proof of Proposition 1 for the pre-activation representations from dense (fully-connected) layers and standard convolutional layers, respectively. The results can be easily extended to other linear neural operators.

Dense layers

Proof. Let $\Omega = \{neu_1, neu_2, \dots, neu_q\}$ denote a dense layer (with q neurons) of any neural network model and H_k denote the pre-activation output of neu_k in Ω . We first provide the theoretical proof to support the observation that H_k tends to follow a normal distribution.

Let $\chi = \mathbb{R}^v$ denote the input feature space (with v features) and assume the feature X_i (which is a random variable) follows a certain distribution $\zeta_i(\mu_i, \sigma_i^2)$ (not necessarily Gaussian) with finite mean $\mu_i = \mathbb{E}[X_i]$ and variance $\sigma_i^2 = \mathbb{E}[X_i - \mu_i]^2$. For each neuron neu_k , let $W_k = [w_{k,1} \ w_{k,2} \ \dots \ w_{k,v}]$ denote the neuron's weight vector, b_k denote the bias, and $Z_{k,i} = X_i w_{k,i}$ denote the i -th weighted input. Let H_k denote the output of neu_k . During the forward propagation, we have:

$$\begin{aligned} H_k &= XW_k^T + b_k \\ &= \sum_{i=1}^v X_i w_{k,i} + b_k \\ &= \sum_{i=1}^v Z_{k,i} + b_k. \end{aligned} \tag{17}$$

Apparently $Z_{k,i}$ is a random variable because $Z_{k,i} = X_i w_{k,i}$ (where the weights $w_{k,i}$ are constants during a forward pass), thus H_k is also a random variable according to Eq. (17).

In an ideal situation, the inputs variables X_1, X_2, \dots, X_v may follow a multivariate normal distribution, in which case Proposition 1 automatically holds due to the property of multivariate normal distribution that every linear combination of the components of the random vector $(X_1, X_2, \dots, X_v)^T$ follows a normal distribution [59]. In other words, $H_k = X_1 w_{k,1} + X_2 w_{k,2} + \dots + X_v w_{k,v} + b_k$ is a normally distributed variable since $w_{k,i}$ and b_k ($k = 1, 2, \dots, v$) are constants in the forward propagation. A special case for this condition is that X_1, X_2, \dots, X_v are independent on each other and X_i follows a normal distribution $\mathcal{N}(\mu_i, \sigma_i^2)$ for all $i = 1, 2, \dots, v$. In this case, by the definition of $Z_{k,i}$, we have:

$$Z_{k,i} = X_i w_{k,i} \sim \mathcal{N}(w_{k,i} \mu_i, (w_{k,i} \sigma_i)^2), \tag{18}$$

where Z_1, Z_2, \dots, Z_v are independent of each other. Combining Eqs. (17) and (18), we have:

$$H_k \sim \mathcal{N}\left(\sum_{i=1}^v w_{k,i} \mu_i + b_k, \sum_{i=1}^v (w_{k,i} \sigma_i)^2\right), \tag{19}$$

For more general cases where X_1, X_2, \dots, X_v are not necessarily normally distributed, we assume the weighted inputs $Z_{k,i}$ of the dense layer satisfy the Lyapunov's condition (see *definition 1*). As a result, we have the following according to the Central Limit Theorem (CLT) [60] considering that X_i follows $\zeta_i(\mu_i, \sigma_i^2)$:

$$\frac{1}{s_k} \sum_{i=1}^v (Z_{k,i} - w_{k,i} \mu_i) \xrightarrow{d} \mathcal{N}(0, 1) \tag{20}$$

where $s_k = \sqrt{\sum_{i=1}^v (w_{k,i} \sigma_i)^2}$ and $\mathcal{N}(0, 1)$ denotes the standard normal distribution. Equivalently, for every neu_k we have:

$$\sum_{i=1}^v Z_{k,i} \xrightarrow{d} \mathcal{N}\left(\sum_{i=1}^v w_{k,i} \mu_i, s_k^2\right) \tag{21}$$

Combining Eqs. (17) and (21) we can derive that:

$$H_k \xrightarrow{d} \mathcal{N}\left(\sum_{i=1}^v w_{k,i} \mu_i + b_k, s_k^2\right), \quad (22)$$

which means that $H_k (k = 1, 2, \dots, v)$ tend to follow a normal distribution and proves our Proposition 1 for fully-connected layers. \square

Convolutional layers

Proof. Standard convolution in CNNs is also a linear transformation of the input feature space and its main difference from dense layers rests on the restricted size of receptive field. Without loss of generality, we analyze the representation (output) of a single kernel. To facilitate our analysis for convolutional layers, let C denote the number of input channels and K denote the kernel size. For ease of presentation, we define a receptive field mapping function $\Theta(k, i, j)$ that maps the positions (k for channel index, i and j for indices on the same channel) of elements in the feature map (i.e., the representations) to the input features. For the k -th kernel, let W_k denote its weight tensor (with $W_{k,c}$ being the weight matrix for channel c) and b_k its bias.

Given the corresponding input patch $X_{\Theta(k,i,j)}$, The element $H_{k,i,j}$ of the representations from a convolutional layer can be formulated as:

$$H_{k,i,j} = \sum_{c=1}^C \sum_{i'=1}^K \sum_{j'=1}^K \left(X_{\Theta(k,i,j)} \circ W_{k,c} \right)_{i',j'} + b_k, \quad (23)$$

where \circ denotes Hadamard product. The three summations reduce the results of element-wise product between the input patch and the k -th kernel to the correspond representation element $H_{k,i,j}$ in the feature map. For ease of presentation, here we use the notation $Z_{c,i',j'}^{(k)}$ to replace $(X_{\Theta(k,i,j)} \circ W_{k,c})_{i',j'}$ and let $\zeta(\mu_{c,i',j'}, \sigma_{c,i',j'}^2)$ be the distribution that $Z_{c,i',j'}^{(k)}$ follows. Note that ζ can be any distribution since we do not make any distributional assumption on $Z_{c,i',j'}^{(k)}$.

With the notations, Eq. (23) can be rewritten in a similar form to Eq. (17):

$$H_{k,i,j} = \sum_{c=1}^C \sum_{i'=1}^K \sum_{j'=1}^K Z_{c,i',j'}^{(k)} + b_k. \quad (24)$$

We use the condition that the random variables $Z_{c,i',j'}^{(k)}$ satisfy the Lyapunov's condition, i.e., there exists a δ such that

$$\lim_{C \times K^2 \rightarrow \infty} \frac{1}{s^{2+\delta}} \sum_{c=1}^C \sum_{i'=1}^K \sum_{j'=1}^K \mathbb{E} \left[|Z_{c,i',j'}^{(k)} - \mu_{c,i',j'}|^{2+\delta} \right] = 0, \quad (25)$$

where $s = \sqrt{\sum_{c=1}^C \sum_{i'=1}^K \sum_{j'=1}^K \sigma_{c,i',j'}^2}$.

Then according to the Lyapunov CLT, the following holds:

$$H_{k,i,j} \xrightarrow{d} \mathcal{N}\left(\sum_{c,i',j' \in \Theta(k,i,j)} \mu_{c,i',j'} + b_k, \sum_{c,i',j' \in \Theta(k,i,j)} \sigma_{c,i',j'}^2\right), \quad (26)$$

which proves our Proposition 1 for standard convolution layers. \square

A.2 Proof of Proposition 2

Without loss of generality, we prove Proposition 2 for the fused representations from the LSTM layer and the residual block of ResNet models, respectively. The results can be easily extended to other non-linear neural operators.

LSTM

Proof. Long Short-Term Memory (LSTM) models are popular for extracting useful representations from sequence data for tasks such as speech recognition and language modeling. Each LSTM layer contains multiple neural units. For the k -th unit, it takes as input the current feature vector $X_t = (X_{t,1}, X_{t,2}, \dots)$, hidden state vector H_{t-1} and its cell state $c_{t-1,k}$. The outputs of the unit are its new hidden state $h_{t,k}$ and cell state $c_{t,k}$. In this paper, we study the distribution of $h_{t,k}$. Multiple gates are adopted in an LSTM unit: by $i_{t,k}$, $f_{t,k}$, $g_{t,k}$ and $o_{t,k}$ we denote the input gate, forget gate, cell gate and output gate of the LSTM unit k at time step t . The update rules of these gates and the cell state are:

$$\begin{aligned} i_{t,k} &= \text{sigmoid}(W_{(i)k}[H_{t-1}, X_t] + b_{(i)k}), \\ f_{t,k} &= \text{sigmoid}(W_{(f)k}[H_{t-1}, X_t] + b_{(f)k}), \\ g_{t,k} &= \tanh(W_{(g)k}[H_{t-1}, X_t] + b_{(g)k}), \\ o_{t,k} &= \text{sigmoid}(W_{(o)k}[H_{t-1}, X_t] + b_{(o)k}), \\ c_{t,k} &= f_{t,k} \cdot c_{t-1,k} + i_{t,k} \cdot g_{t,k}, \end{aligned} \quad (27)$$

where the $W_{(i)k}$, $W_{(f)k}$, $W_{(g)k}$ and $W_{(o)k}$ are the weight parameters and $b_{(i)k}$, $b_{(f)k}$, $b_{(g)k}$ and $b_{(o)k}$ are the bias parameters for the gates.

The output of the LSTM unit $h_{t,k}$ is calculated as the following:

$$h_{t,k} = o_{t,k} \cdot \tanh(c_{t,k}). \quad (28)$$

Using the final hidden states $h_{T,k}$ (with T being the length of the sequence) as the elements of the layer-wise representation, we apply the following layer-wise fusion to further produce H over all the $h_{T,k}$ in a single LSTM layer:

$$H = \sum_{k=1}^d h_{T,k}, \quad (29)$$

where d is the dimension of the LSTM layer. Again, by $\zeta(\mu_k, \sigma_k^2)$ we denote the distribution of $h_{T,k}$ (where the notation T is dropped here since it is typically a fixed parameter). With $\{h_{T,k} | k = 1, 2, \dots, d\}$ satisfying the Lyapunov's condition and by Central Limit Theorem H , tends to follow the normal distribution:

$$H \xrightarrow{d} \mathcal{N}\left(\sum_{i=1}^d \mu_k, \sum_{i=1}^d \sigma_k^2\right), \quad (30)$$

which proves the Proposition 2 for layer-wise fused representations from LSTM. \square

Residual blocks

Proof. Residual blocks are the basic units in the Residual neural network (ResNet) architecture [61]. A typical residual block contains two convolutional layers with batch normalization (BN) and uses the ReLU activation function. The input of the whole block is added to the output of the second convolution (after BN) through a skip connection before the final activation. Since the convolution operators are the same as we formulate in the second part of Section A.1, here we use the notation $\Psi(X)$ to denote the sequential operations of convolution on X followed by BN, i.e., $\Psi(X) \triangleq \text{BN}(\text{Conv}(X))$. Again, we reuse the receptive field mapping $\Theta(k, i, j)$ as defined in Section A.1 to position the inputs

of the residual block corresponding to the element $Z_{k,i,j}$ in the output representation of the whole residual block.

Let X denote the input of the residual block and $Z_{k,i,j}$ denote an element in the output tensor of the whole residual block. Then we have:

$$\begin{aligned} Z_{k,i,j} &= f\left(X_{k,i,j} + BN(Conv(f(BN(Conv(X_{\Theta(k,i,j)}))))))\right) \\ &= f\left(X_{k,i,j} + \Psi(f(\Psi(X_{\Theta(k,i,j)})))\right), \end{aligned} \quad (31)$$

where f is the activation function (ReLU).

We perform channel-wise fusion on the representation from the residual block to produce H_k for the k -th channel:

$$H_k = \sum_{i=1}^{d_H} \sum_{j=1}^{d_W} Z_{k,i,j}, \quad (32)$$

where d_H and d_W are the dimensions of the feature map and k is the channel index.

Let $\zeta(\mu_{k,i,j}, \sigma_{k,i,j}^2)$ denote the distribution that $Z_{k,i,j}$ follows. Then we apply the Lyapunov's condition to the representation elements layer-wise, i.e.,

$$\lim_{d_W \times d_H \rightarrow \infty} \frac{1}{s_k^{2+\delta}} \sum_{i=1}^{d_H} \sum_{j=1}^{d_W} \mathbb{E} [|Z_{k,i,j} - \mu_{k,i,j}|^{2+\delta}] = 0, \quad (33)$$

where $s_k = \sqrt{\sum_{i=1}^{d_H} \sum_{j=1}^{d_W} \sigma_{k,i,j}^2}$.

With the above condition satisfied, by CLT H_k (the fused representation on channel k) tends to follow the normal distribution:

$$H_k \xrightarrow{d} \mathcal{N}\left(\sum_{i=1}^{d_H} \sum_{j=1}^{d_W} \mu_{k,i,j}, \sum_{i=1}^{d_H} \sum_{j=1}^{d_W} \sigma_{k,i,j}^2\right), \quad (34)$$

which proves the Proposition 2 for channel-wise fused representations from any residual block. \square

B Convergence Analysis

In this section we provide the proof of the proposed Theorem 1. The analysis is mainly based on the results provided by [5]. We first introduce several notations to facilitate the analysis.

B.1 Notations

Let U ($|U| = N$) denote the full set of clients and $S(t)$ ($|S(t)| = K$) denote the set of clients selected for participating. By $\theta_k(t)$ we denote the local model on client k at time step t . We define an auxiliary sequence $v_k(t)$ for each client to represent the immediate local model after a local SGD update; $v_k(t)$ is updated from $\theta_k(t-1)$ with learning rate η_{t-1} :

$$v_k(t) = \theta_k(t-1) - \eta_{t-1} \nabla F_k(\theta_k(t-1), \xi_{k,t-1}), \quad (35)$$

where $\nabla F_k(\theta_k(t-1), \xi_{k,t-1})$ is the stochastic gradient computed over a batch of data $\xi_{k,t-1}$ drawn from D_k with regard to $\theta_k(t-1)$.

We also define two virtual sequences $\bar{v}(t) = \sum_{k=1}^N \rho_k v_k(t)$ and $\bar{\theta}(t) = \text{Aggregate}(\{v_k(t)\}_{k \in S(t)})$ for every time step t (Note that the actual global model $\theta(t)$ is only updated at the aggregation steps

$T_A = \{\tau, 2\tau, 3\tau, \dots\}$. Given an aggregation interval $\tau \geq 1$, we provide the analysis for the partial aggregation rule that yields $\bar{\theta}(t)$ as:

$$\bar{\theta}(t) = \frac{1}{K} \sum_{k \in S(t)} v_k(t), \quad (36)$$

where $S(t)$ ($|S(t)| = K$) is the selected set of clients for the round $\lceil \frac{t}{\tau} \rceil$ that contains step t . At the aggregation steps T_A , $\theta(t)$ is equal to $\bar{\theta}(t)$, i.e., $\theta(t) = \bar{\theta}(t)$ if $t \in T_A$.

To facilitate the analysis, we assume each client always performs model update (and synchronization) to produce $v_k(t)$ and $\bar{v}(t)$ (but obviously it does not affect the resulting $\bar{\theta}$ and θ for $k \notin S(t)$).

$$\theta_k(t) = \begin{cases} v_k(t), & \text{if } t \notin T_A \\ \bar{\theta}(t), & \text{if } t \in T_A \end{cases} \quad (37)$$

For ease of presentation, we also define two virtual gradient sequences: $\bar{g}(t) = \sum_{k=1}^N \rho_k \nabla F_k(\theta_k(t))$ and $g(t) = \sum_{k=1}^N \rho_k \nabla F_k(\theta_k(t), \xi_{k,t})$. Thus we have $\mathbb{E}[g(t)] = \bar{g}(t)$ and $\bar{v}(t) = \bar{\theta}(t-1) - \eta_{t-1}g(t-1)$.

B.2 Key Lemmas

To facilitate the proof of our main theorem, we first present several key lemmas.

Lemma 1 (Result of one SGD step). *Under Assumptions 1 and 2 and with $\eta_t < \frac{1}{4L}$, for any t it holds true that*

$$\mathbb{E}\|\bar{v}(t+1) - \theta^*\|^2 \leq (1 - \eta_t \mu) \mathbb{E}\|\bar{\theta}(t) - w^*\|^2 + \eta_t^2 \mathbb{E}\|g_t - \bar{g}_t\|^2 + 6L\eta_t^2 \Gamma + 2\mathbb{E}\left[\sum_{k=1}^N \rho_k \|\theta_k(t) - \bar{\theta}(t)\|^2\right], \quad (38)$$

where $\Gamma = F^* - \sum_{k=1}^N \rho_k F_k^*$.

Lemma 2 (Gradient variance bound). *Under Assumption 3, one can derive that*

$$\mathbb{E}\|g_t - \bar{g}_t\|^2 \leq \sum_{k=1}^N \rho_k^2 \epsilon_k^2. \quad (39)$$

Lemma 3 (Bounded divergence of $w_k(t)$). *Assume Assumption 4 holds and a non-increasing step size η_t s.t. $\eta_t \leq 2\eta_{t+\tau}$ for all $t = 1, 2, \dots$, it follows that*

$$\mathbb{E}\left[\sum_{k=1}^N \rho_k \|\theta_k(t) - \bar{\theta}(t)\|^2\right] \leq 4\eta_t^2 (\tau - 1)^2 G^2. \quad (40)$$

Lemmas 1, 2 and 3 hold for both full and partial participation and are independent of the client selection strategy. We refer the readers to [5] for their proofs and focus our analysis on opportunistic selection.

Let q_k denotes the probability that client k gets selected. Given the optimal penalty factors α_k for $k = 1, 2, \dots, N$ that satisfy $\alpha_k = -\frac{\ln(\Lambda \rho_k)}{\text{div}(RP_k, RP^B)}$, we have $q_k = \frac{\lambda_k}{\Lambda} = \rho_k$ according to Eq. (7). The next two lemmas give important properties of the aggregated model $\bar{\theta}$ as a result of partial participation and non-uniform client selection/sampling.

Lemma 4 (Unbiased aggregation). *For any aggregation step $t \in T_A$ and with $q_k = \rho_k$ in the selection of $S(t)$, it follows that*

$$\mathbb{E}_{S(t)}[\bar{\theta}(t)] = \bar{v}(t). \quad (41)$$

Proof. First, we present a key observation given by [5] as an important trick to handle the randomness caused by client selection with probability distribution $\{q_k\}_{k=1}^N$. By taking the expectation over $S(t)$, it follows that

$$\mathbb{E}_{S(t)} \sum_{k \in S(t)} X_k = K \mathbb{E}_{S(t)}[X_k] = K \sum_{k=1}^N q_k X_k. \quad (42)$$

Let $q_k = \rho_k$, take the expectation of $\bar{\theta}(t)$ over $S(t)$ and notice that $\bar{v}(t) = \sum_{k \in U} \rho_k v_k(t)$:

$$\begin{aligned} \mathbb{E}_{S(t)}[\bar{\theta}(t)] &= \mathbb{E}_{S(t)} \left[\frac{1}{K} \sum_{k \in S(t)} v_k(t) \right] \\ &= \frac{1}{K} \mathbb{E}_{S(t)} \left[\sum_{k \in S(t)} [v_k(t)] \right] \\ &= \frac{1}{K} K \mathbb{E}_{S(t)}[v_k(t)] \\ &= \sum_{k \in U} q_k v_k(t) \\ &= \bar{v}(t). \end{aligned}$$

□

Lemma 5 (Bounded variance of $\bar{\theta}(t)$). *For any aggregation step $t \in T_A$ and with a non-increasing step size η_t s.t. $\eta_t \leq 2\eta_{t+\tau-1}$, it follows that*

$$\mathbb{E}_{S(t)} \|\bar{\theta}(t) - \bar{v}(t)\|^2 \leq \frac{4}{K} \eta_{t-1}^2 \tau^2 G^2. \quad (43)$$

Proof. First, one can prove that $v_k(t)$ is an unbiased estimate of $\bar{v}(t)$ for any k :

$$\mathbb{E}_{S(t)}[v_k(t)] = \sum_{k \in U} q_k v_k(t) = \bar{v}(t). \quad (44)$$

Then by the aggregation rule $\bar{\theta}(t) = \frac{1}{K} \sum_{k \in S(t)} v_k(t)$, we have:

$$\begin{aligned} \mathbb{E}_{S(t)} \|\bar{\theta}(t) - \bar{v}(t)\|^2 &= \frac{1}{K^2} \mathbb{E}_{S(t)} \|K\bar{\theta}(t) - K\bar{v}(t)\|^2 \\ &= \frac{1}{K^2} \mathbb{E}_{S(t)} \left\| \sum_{k \in S(t)} v_k(t) - \sum_{k=1}^K \bar{v}(t) \right\|^2 \\ &= \frac{1}{K^2} \mathbb{E}_{S(t)} \left\| \sum_{k \in S(t)} (v_k(t) - \bar{v}(t)) \right\|^2 \\ &= \frac{1}{K^2} \left(\mathbb{E}_{S(t)} \sum_{k \in S(t)} \|v_k(t) - \bar{v}(t)\|^2 \right. \\ &\quad \left. + \underbrace{\mathbb{E}_{S(t)} \sum_{i,j \in S(t), i \neq j} \langle v_i(t) - \bar{v}(t), v_j(t) - \bar{v}(t) \rangle}_{=0} \right), \end{aligned} \quad (45)$$

where the second term on the RHS of (45) equals zero because $\{v_k(t)\}_{k \in U}$ are independent and unbiased (see Eq. 44). Further, by noticing $t - \tau \in T_A$ (because $t \in T_A$) which implies that $\theta_k(t - \tau) =$

$\bar{\theta}(t - \tau)$ since the last communication, we have:

$$\begin{aligned}
\mathbb{E}_{S(t)} \|\bar{\theta}(t) - \bar{v}(t)\|^2 &= \frac{1}{K^2} \mathbb{E}_{S(t)} \sum_{k \in S(t)} \|v_k(t) - \bar{v}(t)\|^2 \\
&= \frac{1}{K^2} K \mathbb{E}_{S(t)} \|v_k(t) - \bar{v}(t)\|^2 \\
&= \frac{1}{K} \mathbb{E}_{S(t)} \|(v_k(t) - \bar{\theta}(t - \tau)) - (\bar{v}(t) - \bar{\theta}(t - \tau))\|^2 \\
&\leq \frac{1}{K} \mathbb{E}_{S(t)} \|v_k(t) - \bar{\theta}(t - \tau)\|^2,
\end{aligned} \tag{46}$$

where the last inequality results from $\mathbb{E}[v_k(t) - \bar{\theta}(t - \tau)] = \bar{v}(t) - \bar{\theta}(t - \tau)$ and that $\mathbb{E}\|X - \mathbb{E}X\|^2 \leq \tau \|X\|^2$. Further, we have:

$$\begin{aligned}
\mathbb{E}_{S(t)} \|\bar{\theta}(t) - \bar{v}(t)\|^2 &\leq \frac{1}{K} \mathbb{E}_{S(t)} \|v_k(t) - \bar{\theta}(t - \tau)\|^2 \\
&= \frac{1}{K} \sum_{k=1}^N q_k \mathbb{E}_{S(t)} \|v_k(t) - \bar{\theta}(t - \tau)\|^2 \\
&= \frac{1}{K} \sum_{k=1}^N q_k \underbrace{\mathbb{E}_{S(t)} \left\| \sum_{i=t-\tau}^{t-1} \eta_i \nabla F_k(\theta_k(i), \xi_{k,i}) \right\|^2}_{Z_1}.
\end{aligned} \tag{47}$$

Let $i_m = \arg \max_i \|\nabla F_k(\theta_k(i), \xi_{k,i})\|, i \in [t - \tau, t - 1]$. By using the Cauchy-Schwarz inequality, Assumption 4 and choosing a non-increasing η_t s.t. $\eta_t \leq 2\eta_{t+\tau-1}$, we have:

$$\begin{aligned}
Z_1 &= \mathbb{E}_{S(t)} \left\| \sum_{i=t-\tau}^{t-1} \eta_i \nabla F_k(\theta_k(i), \xi_{k,i}) \right\|^2 \\
&= \sum_{i=t-\tau}^{t-1} \sum_{j=t-\tau}^{t-1} \mathbb{E}_{S(t)} \langle \eta_i \nabla F_k(\theta_k(i), \xi_{k,i}), \eta_j \nabla F_k(\theta_k(j), \xi_{k,j}) \rangle \\
&\leq \sum_{i=t-\tau}^{t-1} \sum_{j=t-\tau}^{t-1} \mathbb{E}_{S(t)} \left[\|\eta_i \nabla F_k(\theta_k(i), \xi_{k,i})\| \cdot \|\eta_j \nabla F_k(\theta_k(j), \xi_{k,j})\| \right] \\
&\leq \sum_{i=t-\tau}^{t-1} \sum_{j=t-\tau}^{t-1} \eta_i \eta_j \cdot \mathbb{E}_{S(t)} \|\nabla F_k(\theta_k(i_m), \xi_{k,i_m})\|^2 \\
&\leq \sum_{i=t-\tau}^{t-1} \sum_{j=t-\tau}^{t-1} \eta_{t-\tau}^2 \cdot \mathbb{E}_{S(t)} \|\nabla F_k(\theta_k(i_m), \xi_{k,i_m})\|^2 \\
&\leq 4\eta_{t-1}^2 \tau^2 G^2.
\end{aligned} \tag{48}$$

Plug Z_1 back into (47) and notice that $\sum_{k=1}^N q_k = 1$, we have:

$$\begin{aligned}
\mathbb{E}_{S(t)} \|\bar{\theta}(t) - \bar{v}(t)\|^2 &\leq \frac{1}{K} \sum_{k=1}^N q_k 4\eta_t^2 \tau^2 G^2 \\
&= \frac{4}{K} \eta_{t-1}^2 \tau^2 G^2.
\end{aligned}$$

□

B.3 Proof of Theorem 1

Proof. Taking expectation of $\|\bar{\theta}(t) - \theta^*\|^2$, we have:

$$\begin{aligned} \mathbb{E}\|\bar{\theta}(t) - \theta^*\|^2 &= \mathbb{E}_{S(t)}\|\bar{\theta}(t) - \bar{v}(t) + \bar{v}(t) - \theta^*\|^2 \\ &= \underbrace{\mathbb{E}\|\bar{\theta}(t) - \bar{v}(t)\|^2}_{A_1} + \underbrace{\mathbb{E}\|\bar{v}(t) - \theta^*\|^2}_{A_2} + \underbrace{\mathbb{E}\langle \bar{\theta}(t) - \bar{v}(t), \bar{v}(t) - \theta^* \rangle}_{A_3} \end{aligned} \quad (49)$$

where A_3 vanishes because $\bar{\theta}(t)$ is an unbiased estimate of $\bar{v}(t)$ by first taking expectation over $S(t)$ (Lemma 4).

To bound A_2 for $t \in T_A$, we apply Lemma 1:

$$\begin{aligned} A_2 = \mathbb{E}\|\bar{v}(t) - \theta^*\|^2 &\leq (1 - \eta_{t-1}\mu)\mathbb{E}\|\bar{\theta}(t-1) - \theta^*\|^2 + \underbrace{\eta_{t-1}^2 \mathbb{E}\|g_{t-1} - \bar{g}_{t-1}\|^2}_{B_1} \\ &\quad + \underbrace{6L\eta_{t-1}^2\Gamma + \mathbb{E}\left[\sum_{k=1}^N \rho_k \|\theta_k(t-1) - \bar{\theta}(t-1)\|^2\right]}_{B_2}. \end{aligned} \quad (50)$$

Then we use Lemmas 2 and 3 to bound B_1 and B_2 respectively, which yields:

$$A_2 = \mathbb{E}\|\bar{v}(t) - \theta^*\|^2 \leq (1 - \eta_{t-1}\mu)\mathbb{E}\|\bar{\theta}(t-1) - \theta^*\|^2 + \eta_{t-1}^2 \mathcal{B}, \quad (51)$$

where $\mathcal{B} = \sum_{k=1}^N \rho_k^2 \epsilon_k^2 + 6L\Gamma + 8(\tau-1)^2 G^2$.

To bound A_1 , one can first take expectation over $S(t)$ and apply Lemma 5 where the upper bound actually eliminates both sources of randomness. Thus, it follows that

$$A_1 = \mathbb{E}\|\bar{\theta}(t) - \bar{v}(t)\|^2 \leq \frac{4}{K} \eta_{t-1}^2 \tau^2 G^2 \quad (52)$$

Let $\mathcal{C} = \frac{4}{K} \tau^2 G^2$ and plug A_1 and A_2 back into (49):

$$\mathbb{E}\|\bar{\theta}(t) - \theta^*\|^2 \leq (1 - \eta_{t-1}\mu)\mathbb{E}\|\bar{\theta}(t-1) - \theta^*\|^2 + \eta_{t-1}^2 (\mathcal{B} + \mathcal{C}). \quad (53)$$

Equivalently, let $\Delta_t = \mathbb{E}\|\bar{\theta}(t) - \theta^*\|^2$, then we have the following recurrence relation for any $t \geq 1$:

$$\Delta_t \leq (1 - \eta_{t-1}\mu)\Delta_{t-1} + \eta_{t-1}^2 (\mathcal{B} + \mathcal{C}). \quad (54)$$

Next we prove by induction that $\Delta_t \leq \frac{\nu}{\gamma+t}$ where $\nu = \max\left\{\frac{\beta^2(\mathcal{B}+\mathcal{C})}{\beta\mu-1}, (\gamma+1)\Delta_1\right\}$ using an aggregation interval $\tau \geq 1$ and a diminishing step size $\eta_t = \frac{\beta}{t+\gamma}$ for some $\beta > \frac{1}{\mu}$ and $\gamma > 0$ such that $\eta_1 \leq \min\{\frac{1}{\mu}, \frac{1}{4L}\}$ and $\eta_t \leq 2\eta_{t+\tau}$.

First, for $t = 1$ the conclusion holds that $\Delta_1 \leq \frac{\nu}{\gamma+1}$ given the conditions. Then by assuming it holds for some t , one can derive from (54) that

$$\begin{aligned} \Delta_{t+1} &\leq (1 - \eta_t\mu)\Delta_t + \eta_t^2 (\mathcal{B} + \mathcal{C}) \\ &\leq \left(1 - \frac{\beta\mu}{t+\gamma}\right) \frac{\nu}{\gamma+t} + \left(\frac{\beta}{t+\gamma}\right)^2 (\mathcal{B} + \mathcal{C}) \\ &= \frac{t+\gamma-1}{(t+\gamma)^2} \nu + \underbrace{\left[\frac{\beta^2(\mathcal{B}+\mathcal{C})}{(t+\gamma)^2} - \frac{\beta\mu-1}{(t+\gamma)^2} \nu\right]}_{\geq 0} \\ &\leq \frac{t+\gamma-1}{(t+\gamma)^2} \nu \\ &\leq \frac{t+\gamma-1}{(t+\gamma)^2-1} \nu \\ &= \frac{\nu}{t+\gamma+1}, \end{aligned} \quad (55)$$

which proves the conclusion $\Delta_t \leq \frac{\nu}{\gamma+t}$ for any $t \geq 1$.

Then by the smoothness of the objective function F , it follows that

$$\begin{aligned} \mathbb{E}[F(\bar{\theta}(t))] - F^* &\leq \frac{L}{2} \mathbb{E}[\|\bar{\theta}(t) - \theta^*\|^2] \\ &= \frac{L}{2} \Delta_t \leq \frac{L}{2} \frac{\nu}{\gamma+t}. \end{aligned} \quad (56)$$

Specifically, by choosing $\beta = \frac{2}{\mu}$ (i.e., $\eta_t = \frac{2}{\mu(\gamma+t)}$), $\gamma = \max\{\frac{8L}{\mu}, \tau\} - 1$, we have

$$\begin{aligned} \nu &= \max\left\{\frac{\beta^2(\mathcal{B} + \mathcal{C})}{\beta\mu - 1}, (\gamma + 1)\Delta_1\right\} \\ &\leq \frac{\beta^2(\mathcal{B} + \mathcal{C})}{\beta\mu - 1} + (\gamma + 1)\Delta_1 \\ &= \frac{4(\mathcal{B} + \mathcal{C})}{\mu^2} + (\gamma + 1)\Delta_1. \end{aligned} \quad (57)$$

By definition, we have $\theta(t) = \bar{\theta}(t)$ at the aggregation steps. Therefore, for $t \in T_A$:

$$\begin{aligned} \mathbb{E}[F(\theta(t))] - F^* &\leq \frac{L}{2} \frac{\nu}{\gamma+t} \\ &= \frac{L}{(\gamma+t)} \left(\frac{2(\mathcal{B} + \mathcal{C})}{\mu^2} + \frac{\gamma+1}{2} \Delta_1 \right). \end{aligned}$$

□

C Profile Dissimilarity under Homomorphic Encryption

The proposed representation profiling scheme encodes the representations of data into a list of distribution parameters, namely $RP(\theta, D) = \{(\mu_i, \sigma_i^2) | i = 1, 2, \dots, q\}$ where q is the length of the profile. Theoretically, the information leakage (in terms of the data in D) by exposing $RP(\theta, D)$ is very limited and it is basically impossible to reconstruct the samples in D given $RP(\theta, D)$. Nonetheless, Homomorphic Encryption (HE) can be applied to the profiles (both locally and on the server) so as to guarantee zero knowledge disclosure while still allowing profile matching under the encryption. In the following we give details on how to encrypt a representation profile and compute profile dissimilarity under Homomorphic Encryption (HE).

To calculate (3) and (4) under encryption, a client needs to encrypt (denoted as $[[\cdot]]$) every single μ_i and σ_i^2 in its profile $RP_k(\theta, D_k)$ locally before upload whereas the server does the same for its $RP^B(\theta, D^V)$. Therefore, according to Eq. (4) we have:

$$\begin{aligned} [[\text{KL}(\mathcal{N}_i^{(k)} || \mathcal{N}_i^B)]] &= \frac{1}{2} \log[[(\sigma_i^B)^2]] - \frac{1}{2} \log[[(\sigma_i^{(k)})^2]] - [[\frac{1}{2}]] \\ &\quad + \frac{([[(\sigma_i^{(k)})^2]] + ([[\mu_i^{(k)}]] - [[\mu_i^B]])^2)}{2[[(\sigma_i^B)^2]]}, \end{aligned} \quad (58)$$

where the first two terms on the right-hand side require logarithm operation on the ciphertext. However, this may not be very practical because most HE schemes are designed for basic arithmetic operations on the ciphertext. Thus we also consider the situation where HE scheme at hand only provides *additive and multiplicative* homomorphisms [62]. In this case, to avoid the logarithm operation, the client k needs to keep every σ_i^2 in $RP_k(\theta, D_k)$ as plaintext and only encrypts μ_i , likewise for the

server. As a result, the KL divergence can be computed under encryption as:

$$\begin{aligned}
[[\text{KL}(\mathcal{N}_i^{(k)} || \mathcal{N}_i^B)]] &= \left[\left[\frac{1}{2} \log\left(\frac{\sigma_i^B}{\sigma_i^{(k)}}\right)^2 + \frac{1}{2} \left(\frac{\sigma_i^{(k)}}{\sigma_i^B}\right)^2 - \frac{1}{2} \right] \right] \\
&\quad + \frac{1}{2(\sigma_i^B)^2} ([[\mu_i^{(k)}]] - [[\mu_i^B]])^2
\end{aligned} \tag{59}$$

where the first term on the right-hand side is encrypted after calculation with plaintext values $(\sigma_i^k)^2$ and $(\sigma^B)^2$ whereas the second term requires multiple operations on the ciphertext values $[[\mu_i^k]]$ and $[[\mu^B]]$.

Now, in either case, we can compute profile dissimilarity under encryption by summing up all the KL divergence values in ciphertext:

$$[[div(RP_k, RP^B)]] = \frac{1}{q} \sum_{i=1}^q [[\text{KL}(\mathcal{N}_i^{(k)} || \mathcal{N}_i^B)]] \tag{60}$$